Experimental measurement of ^{91}Zr$(n,\gamma)^{92}$Zr at the CSNS Back-n facility from 0.82 keV to 229 keV

L. Gan,[1] H. B. Sun,[2,3] W. Jiang,[4,5] Z. H. Li,[6,7,*] J. Zhong,[8] A. Rohilla,[9] Z. Y. Huang,[10] X. Y. Li,[11] W. Nan,[6] W. K. Nan,[6] S. P. Hu,[2,3] and E. T. Li[12]

[1]*Shenzhen Institute of Information Technology, Shenzhen 518172, China*
[2]*Institute for Advanced Study in Nuclear Energy and Safety, Shenzhen University, Shenzhen 518060, China*
[3]*Shenzhen Key Laboratory of Research and Manufacture of High Purity Germanium Materials and Detectors, Shenzhen University, Shenzhen 518060, China*
[4]*Spallation Neutron Source Science Center, Dongguan 523803, China*
[5]*Institute of High Energy Physics, Chinese Academy of Sciences, Beijing 100049, China*
[6]*China Institute of Atomic Energy, P.O. Box 275(10), Beijing 102413, China*
[7]*Jinping Deep Underground Frontier Science and Dark Matter Key Laboratory of Sichuan Province, Liangshan 615000, China*
[8]*College of Engineering Physics, Shenzhen Technology University, Shenzhen 518118, China*
[9]*Department of Physics and Astronomy, CMS Collaboration, University of Nebraska-Lincoln, Nebraska 68508, USA*
[10]*Origin Quantum Computing Technology (Hefei) Co., Ltd., HeFei 230093, China*
[11]*Institute of Modern Physics, Fudan University, Shanghai 200433, China*
[12]*College of Physics and Optoelectronic Engineering, Shenzhen University, Shenzhen 518060, China*

(Received 27 April 2024; revised 23 June 2024; accepted 29 July 2024; published 15 August 2024)

Zr isotopes are important nuclides on the *s*-process path, and their neutron capture cross sections are of great significance for studying the evolution of heavy nuclei in the universe. In this work, the cross section of the ^{91}Zr$(n,\gamma)^{92}$Zr reaction was measured at the China Spallation Neutron Source (CSNS) Back-n platform from 0.82 keV to 229 keV, essentially covering the energy range of astrophysical interest. In the experiment, a high-purity germanium detector with excellent energy resolution was used, which allowed for the accurate identification of characteristic γ rays emitted during ^{92}Zr's de-excitation, thereby enabling precise measurement of the neutron capture cross section. Furthermore, the measurement yielded the Maxwellian-averaged cross section of 56.4 ± 5.0 mb calculated at $kT = 30$ keV.

DOI: 10.1103/PhysRevC.110.025802

I. INTRODUCTION

Due to the formidable Coulomb barrier, elements heavier than iron are difficult to be produced through the capture of charged particles. Existing research indicates that most heavy elements above iron are formed through the capture of electrically neutral neutrons by seed nuclei [1]. Based on the timescale of neutron capture, these reaction paths are classified as slow (*s* process) and rapid (*r* process) neutron capture processes. It is now widely accepted that both contribute approximately half of the heavy nuclides. The *s* process primarily occurs in asymptotic giant branch (AGB) stars, with typical temperatures ranging from 1.5 to 4×10^8 K, corresponding to the temperature of helium burning in AGB stars. Under these conditions, neutron energies typically range from 10 to 32 keV [1–7]. The interval between two neutron capture events can range from several years to several centuries, allowing unstable nuclei on the *s*-process path ample time to undergo β decay and become stable or long-lived nuclei.

Zr plays a crucial role in the main *s* process and exhibits remarkable stability, with a proton number equal to 40 and neutrons around 50. This leads to a relatively lower neutron capture cross section compared to nearby elements, making them bottleneck reactions on the *s*-process path. By studying the neutron capture reactions of Zr isotopes, researchers can gain insights into the formation and evolution of stars, synthesis of elements in the universe, and the conditions within astrophysical sites [8–11].

In the past 60 years, several experimental efforts have been made to measure the neutron capture reaction of ^{91}Zr [9,12–15]. A representative work was published by Tagliente *et al.* in 2008 [9], where they measured the γ rays generated from the reaction between a neutron beam and a ZrO_2 target enclosed in an aluminum can using a C_6D_6 detector array, where 'D' denotes '^{2}H', at the n_TOF facility at CERN. The amount of γ rays recorded by C_6D_6 represents the yield of the total reaction cross section of $n + {}^{91}$Zr. Then, the neutron capture reaction cross section ratio was determined through weighting functions [16]. However, this measurement method is inevitably subjected to interference from various uncertain factors. First, the reaction target was ZrO_2 powder enclosed in an aluminum shell. Among the measured γ rays, the effect of neutrons interacting with oxygen and aluminum presented the

*Contact author: zhli@ciae.ac.cn

non-negligible contributions. Although the effect of aluminum can be deducted independently by measuring the $n+$ Al target cross section, although it is difficult to completely neglect the effect due to $n+$O yield. Second, the content of ^{91}Zr in the reaction target is approximately 90%, and the remaining 10% indicates the effect due to other Zr isotopes interfering with the experimental data. Third, it can be seen from previously published experimental data that the cross section measurements in the resonance energy region are relatively flat. This is because the measured reaction yield is the overall effect of multiple different reactions, and interference among them can mask the characteristics of the neutron capture reaction of ^{91}Zr. Finally, due to the weak γ energy resolution of the C_6D_6 detector, these disadvantages cannot be overcome.

The state of ^{92}Zr generated by the neutron capture reaction of ^{91}Zr has two conditions: either through direct radiation capture reaction to the ground state or through occupancy of different excited states. Since the ground state spin-parity of ^{92}Zr is 0^+, the excited states with spins of 1 and 2 are most likely to de-excite directly to the ground state. These excited states are the first (934.5 keV 2^+), the fourth (1847.3 keV 2^+), and several higher excited states with excitation energies between 2819.5 keV and 3915 keV [17,18]. Therefore, the cross section of the ^{91}Zr$(n,\gamma)^{92}$Zr reaction can be determined by measuring the γ rays of these specific transitions. Reference [17] shows the γ rays emitted from ^{92}Zr produced by the reaction of ^{91}Zr with thermal neutrons. Among these, the 934.5 keV γ ray has an extremely high intensity, accounting for 79% of the total intensity. The intensity of the 1847.3 keV γ ray is about 5% of that of the total reaction yields. It is worth noting that the 1847.3 keV state emits two γ rays: 912.7 keV ($I = 100$) and 1847.3 keV ($I = 51$). To reduce statistical error, the statistics of the 912.7 keV γ ray were used to deduce those of the 1847.3 keV γ ray here. The remaining γ rays of interest have very weak intensities, totaling about 3.3% of the total reaction yields. Hence, the 934.5 keV γ ray is particularly noteworthy, however, the other γ rays cannot be ignored either. Based on the decay scheme of ^{92}Zr, this work introduced a novel approach to measuring the neutron capture cross section of ^{91}Zr by using a high-purity germanium (HPGe) detector, which provides better resolution and accuracy compared to previous methods. In the discussion part of the paper, we calculated the Maxwellian-averaged cross section (MACS) using the cross section data measured in this study.

The Back-n white neutron source at China Spallation Neutron Source (CSNS), located in southern China, can provide a continuous neutron beam with an energy range from 0.3 eV to 300 MeV. This experimental platform primarily serves the purpose of measuring neutron capture cross sections. The neutrons are generated through the bombardment of a spallation target by a proton beam with an energy of 1.6 GeV and a frequency of 25 Hz. At distances of 55 m and 76 m from the spallation target, two end stations, ES#1 and ES#2, have been set up, respectively [19–22]. The Back-n beam line features one shutter and two collimators, enabling the shaping of the beam profile into various sizes by adjusting the apertures of the shutter and collimators. The neutron beam intensity within the energy range (about 30 keV) of interest to astrophysics can reach up to 10^4 n/(cm^2 s) [20–24].

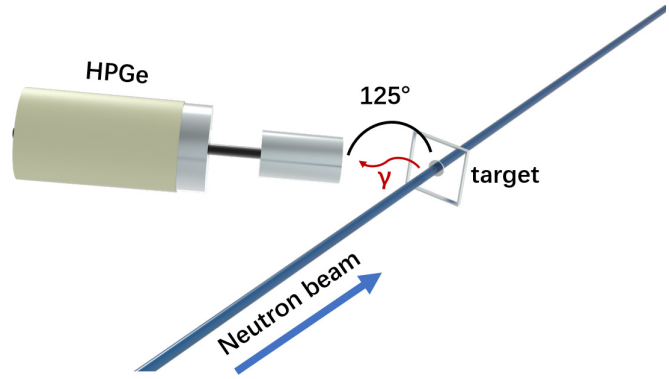

FIG. 1. Experimental setup: HPGe detector mounted at 125 angles to the beam direction, with a ^{nat}Zr target positioned along the center of the neutron beam axis.

II. EXPERIMENT

In this experiment, conducted at the ES#2 end-station, we were conscious of the potential impact of high neutron beam intensities on the detector system, specifically concerning the increase in dead time. High-intensity neutron beams can cause prolonged dead times in detection systems, which may distort or lose critical data within the target energy region. To mitigate this issue and to ensure that data collection was not affected by excessive dead times, we employed the smallest possible shutter setting in our experimental setup. Consequently, the neutron beam intensity utilized in this study was an order of magnitude lower than optimal conditions, which helped us in preserving the integrity of our measurements while potentially affecting the overall neutron flux captured during the experiment.

As shown in Fig. 1, a ^{nat}Zr target with an abundance of ^{91}Zr at 11.23%, has a diameter of 30 mm and a thickness of 7.8 mm, was placed at the center of the neutron beam line, perpendicular to the beam direction. An HPGe detector was positioned 202 mm behind and to the left of the experimental target, forming a 125-degree angle with the beam direction, to detect the γ rays emitted during the reaction. As the detection efficiency of the detector at 934.3 keV is approximately 0.0048%, to ensure sufficient statistics, we conducted experimental measurements totaling over 160 h. The energy and efficiency calibration of the detector were performed using the standard radioactive sources, specifically ^{60}Co and ^{152}Eu.

III. EXPERIMENTAL RESULTS AND ANALYSIS

During the standard operation mode of the CSNS, each pulse comprises of two proton bunches separated by a time interval of 410 ns. The moment when the first proton beam bunch hits the target is taken as the starting point for the time of flight recorded by the detector. To accurately analyze the γ-ray yield contributed by each beam bunch mathematically, both the start point of the neutron flight time and the length

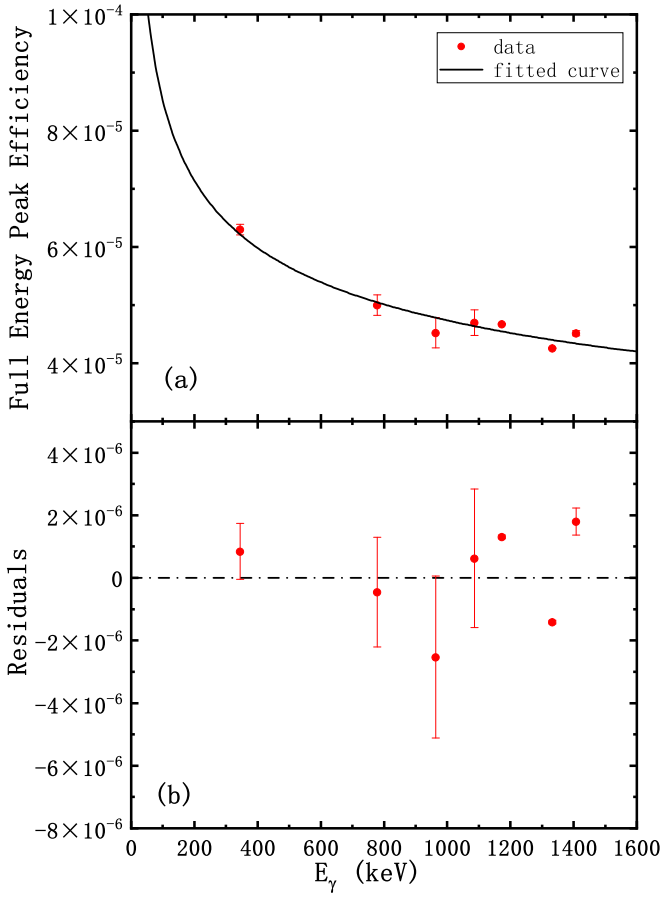

FIG. 2. The full energy peak efficiency of HPGe detector and residuals of the fitted curve. (a) The red dots with error bars represent the experimental data, and the black line represents the fitted efficiency curve. (b) shows the residual distribution of the data points corresponding to the fitted curve.

of the time window were chosen as multiples of 410 ns in the following processes. To fully measure the experimental data within the energy range of interest in astrophysics the start and end points of the flight time are set at 11,480 ns and 19,1880 ns, respectively, corresponding to a neutron energy range from 0.82 keV to 229 keV.

A. Calibration and efficiency of HPGe

In this work, two standard radioactive sources, ^{60}Co and ^{152}Eu, were utilized. Seven γ rays, 344.3 keV, 778.9 keV, 964.1 keV, 1085.8 keV, 1173.2 keV, 1332.5 keV, and 1408.1 keV, were adopted to calibrate the energy and detection efficiency of the HPGe detector. Figure 2 displays the results of energy efficiency calibration for the HPGe detector. The functional expression of energy efficiency fitted by using the experimental data is as follows:

$$\lg(\epsilon) = -0.255(\pm 0.03)\lg(E_\gamma) - 3.559(\pm 0.09), \quad (1)$$

where E_γ is in keV.

B. Double-bunch unfolding method

For the convenience of description, let us name the two beam bunches as bunch A and bunch B. It is natural to assume that bunch A and bunch B have the same neutron energy spectrum. Furthermore, there is a time interval of 410 ns between bunch A and bunch B. Taking 410 ns as the unit time, which corresponds to the time gap between the two consecutive beam bunches. During the first unit time, the data recorded by the detector were entirely produced by bunch A. However, the situation changes during the second unit time. The experimental results include data from bunch A during the second unit time combined with data from bunch B during the first unit time. This pattern continues so that during the nth unit time, the data recorded by the detector is derived from the γ rays produced by bunch A during the nth unit time and by bunch B during the $(n-1)$th unit time. Let $f(n)$ represent the actual reaction yield of a single beam bunch during the nth unit time, and let $A(n)$ represent the reaction yield measured by the detector during the nth unit time. Then, the relationship between $f(n)$ and $A(n)$ is as follows:

$$\begin{aligned} A(1) &= f(1), \\ A(2) &= f(1) + f(2), \\ A(3) &= f(2) + f(3), \\ &\vdots \\ A(n) &= f(n-1) + f(n) \quad (n > 1). \end{aligned} \quad (2)$$

Additionally, to reduce statistical errors, it is necessary to ensure that each time window has sufficient statistics of reaction yield, therefore a time duration of 4100 ns is selected. Assuming that the starting point of the time of flight (TOF) for a certain energy range is the xth unit time, then its ending point would be the $(x+9)$th unit time. One can derive that

$$Count = f(x+0) + f(x+1) + \cdots + f(x+9). \quad (3)$$

According to Eq. (2)

$$\begin{aligned} f(x+0) + f(x+1) &= A(x+1), \\ f(x+2) + f(x+3) &= A(x+3), \\ &\vdots \\ f(x+8) + f(x+9) &= A(x+9). \end{aligned} \quad (4)$$

Combining Eqs. (3) and (4), the expression of *count* can be rewritten as

$$\begin{aligned} Count = {} & A(x+1) + A(x+3) + A(x+5) \\ & + A(x+7) + A(x+9). \end{aligned} \quad (5)$$

By integrating the corresponding data from the above equation into a new data set, we can successfully extract the actual numerical value of the *count*.

C. Data analysis

The TOF range for neutrons analyzed in this work extended from 11 480 ns to 19 1880 ns. In processing the data, the

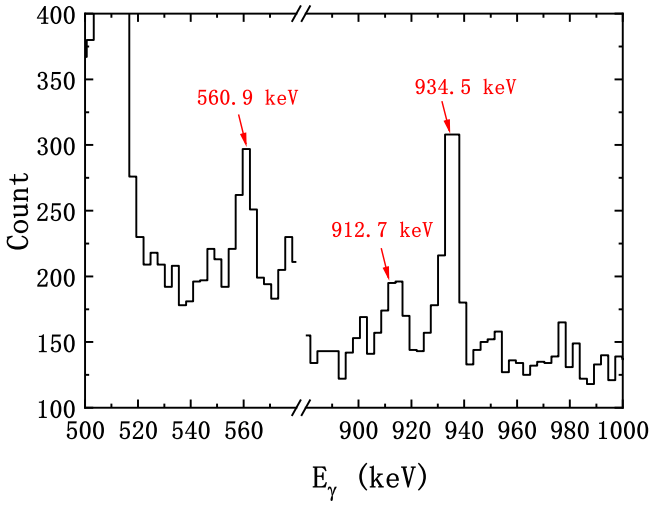

FIG. 3. The energy spectrum of an HPGe detector with the incident neutron energy is 2.6 keV. The energy peaks at 560.9 keV, 912.7 keV, and 934.3 keV were marked with red arrows.

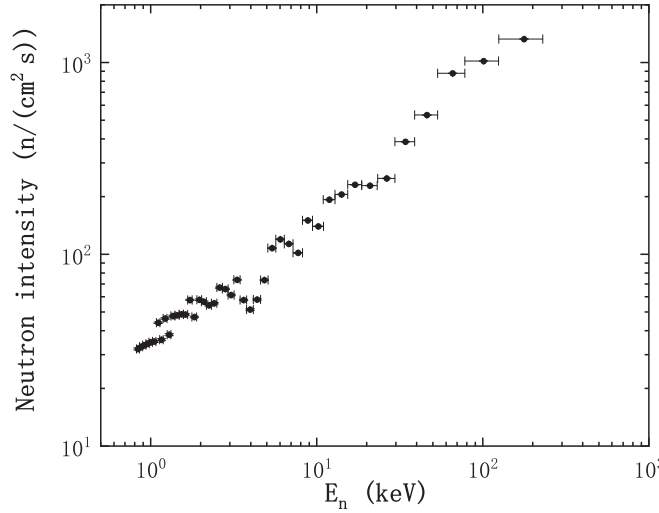

FIG. 4. The neutron intensity under the present experimental setup. The data points represent the total neutron intensity within each energy interval, with the maximum relative error being approximately 1%.

entire time range was first divided into 440 parts with 410 ns intervals. These 440 sets of data were then grouped into 44 groups, each consisting of ten sets. According to Eq. (5), the sets numbered with even indices within each group represent the reaction yields of individual beam bunches within the corresponding energy range.

As shown in Fig. 3, the energy spectrum of the detector is in the range of 500 keV to 1000 keV when the incident neutron energy is 2.6 keV. Within it, the γ energy peaks at 560.9 keV, 912.7 keV, and 934.3 keV from ^{91}Zr can be easily identified. The 560.9 keV γ ray comes from the 1495.5 keV $(4^+) \rightarrow$ 934.5 keV (2^+) transition. Since the 1495.5 keV state can only emit this γ ray, it does not affect the cross section. Therefore, the yield of the ^{91}Zr$(n,\gamma)^{92}$Zr was represented by the sum of the statistics of the 934.5 keV γ ray and half of the statistics of the 912.7 keV γ ray. The actual statistics are derived by subtracting the baseline height from the peak area here. The contribution comes from several highly excited states that can directly de-excite to the ground state. According to the data in Ref. [17], their contribution is approximately 3.3%. However, due to their low individual intensities and the lower detection efficiency of the HPGe detector at this energy zone, they were not identified in this experiment. Therefore, a correction factor of 3.3% was applied to the final cross section data to account for the contributions of the remaining possible de-excitation paths. Additionally, introduce 3.3% as the uncertainty contributed by them into the error analysis of the final cross section. Then, the reaction cross section within this neutron energy range can be obtained:

$$\sigma = \frac{count}{N_{^{91}Zr} \cdot I_n \cdot t \cdot \epsilon} \tag{6}$$

In Eq. (6), $N_{^{91}Zr}$ represents the number of ^{91}Zr atoms, I_n denotes the neutron beam intensity $[n/(\mathrm{cm}^2\ \mathrm{s})]$, t indicates the measurement time, and ϵ represents the detection efficiency of the detector for characteristic γ rays, respectively. The neutron beam intensity is provided by CSNS [23,24], and is shown in Fig. 4. After individually processing the data for each group, reaction cross sections for 44 different energy intervals were obtained.

From Fig. 5, it can be seen that the neutron capture cross section of ^{91}Zr exhibits significant oscillations as a function of the incident neutron energy, particularly in the energy range below 10 keV.

The averaged neutron capture cross section of ^{91}Zr is listed in Table I.

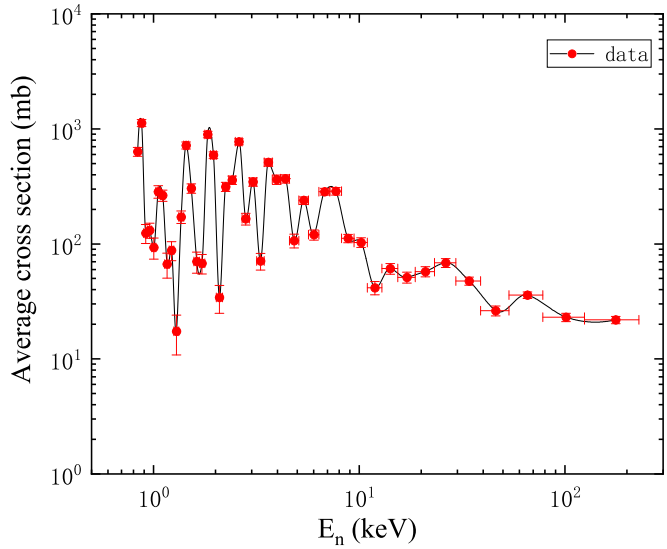

FIG. 5. The averaged cross sections of ^{91}Zr$(n,\gamma)^{92}$Zr reaction with the neutron energy from 0.82 keV to 229 keV. The curve is merely to illustrate the trend of data changes and does not represent calculated values.

TABLE I. Averaged neutron capture cross sections of ^{91}Zr.

E_{min} keV	E_{max} keV	σ mb	$\Delta\sigma$ mb
0.86	0.82	1009.4	82
0.89	0.86	1166.8	91
0.94	0.89	118.1	23
0.98	0.94	136.1	21
1.03	0.98	96.3	20
1.08	1.03	197.8	28
1.13	1.08	272.8	32
1.19	1.13	157.7	26
1.26	1.19	171.6	25
1.33	1.26	18	6.9
1.4	1.33	177.8	23
1.48	1.4	743.3	58
1.57	1.48	314.6	32
1.67	1.57	72.6	15
1.78	1.67	60.1	12
1.89	1.78	924.8	66
2.02	1.89	611.8	47
2.17	2.02	29	8.7
2.32	2.17	325.4	32
2.5	2.32	371.6	33
2.7	2.5	735.7	50
2.92	2.7	146.2	18
3.17	2.92	357.7	32
3.45	3.17	69.2	12
3.78	3.45	528.7	42
4.15	3.78	334.5	33
4.58	4.15	381.7	34
5.08	4.58	110.6	16
5.67	5.08	247	20
6.36	5.67	97.7	11
7.19	6.36	294.5	22
8.2	7.19	271.2	22
9.43	8.2	115.6	10
10.96	9.43	106.7	11
12.9	10.96	75.5	7.9
15.4	12.9	63.1	7.1
18.7	15.4	48	5.3
23.19	18.7	77.4	7.3
29.52	23.19	100.7	8.2
38.84	29.52	62.9	5.3
53.39	38.84	27.1	2.8
77.95	53.39	37.2	2.7
124.37	77.95	19	1.8
229.07	124.37	20.1	1.6

D. Direct radiation capture reaction cross section

As we mentioned in the Iintroduction, there are two situations for the neutron capture reaction of ^{91}Zr. The first situation involves the direct radiative capture of ^{91}Zr to form the ground state of ^{92}Zr. The second situation results in the formation of an excited state of ^{92}Zr, which then decays to the ground state. The experimental method of this work measures the γ rays emitted from the second situation. To completely obtain the total reaction cross section, it is also necessary to consider the cross section of the first situation.

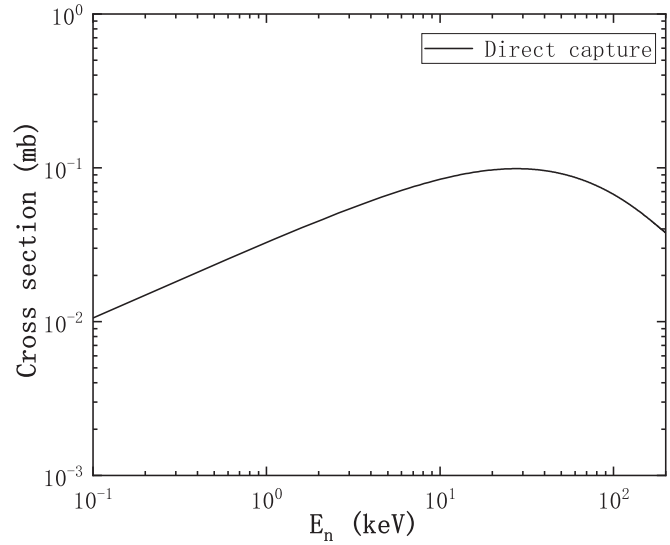

FIG. 6. The theoretical direct radiation neutron capture reaction cross section of ^{91}Zr to the ground state of ^{92}Zr.

The RADCAP nuclear physics calculation program [25] was used to compute the cross sections of this reaction. During the calculation process, the neutron spectroscopic factor for ^{91}Zr was set to 1.75 [26]. The direct radiative capture cross section for neutron incident energies ranging from 0.1 keV to 300 keV is shown in Fig. 6. The ratio of the direct radiative capture cross section versus the experimental measurement results is less than 0.6% across the entire energy range., thus the direct radiative capture cross section can be ignored.

E. Error analysis

From Eq. (6), it is evident that the uncertainties in the reaction cross section are driven by the statistics of the characteristic γ rays, the atomic amount of ^{91}Zr, the neutron beam intensity, the measurement duration, the energy efficiency of HPGe detector, and the effects of several other possible decay paths of ^{92}Zr. Specifically,

(1) The statistical error of the characteristic γ rays predominantly ranges between 5% and 10%, with some errors exceeding 20%. These data points are all located at the bottom of the resonance region.
(2) The atomic amount of ^{91}Zr is determined by the mass of the zirconium metal target and the natural abundance of ^{91}Zr. The target mass was repeatedly measured using a high-precision electronic scale and averaged, with errors less than 0.01%, which is negligible.
(3) The error in neutron intensity is based on data provided by CSNS. Its relative error decreases gradually with increasing neutron incident energy, with a maximum value of approximately 1%. The impact is therefore quite limited.
(4) The error due to measurement time is about 0.1% and can be disregarded.
(5) The error introduced by the detector energy efficiency curve is approximately 2.5%.

TABLE II. MACS values at $kT = 30$ keV thermal energy.

MACS (mb)	Ref.	year
59 ± 10[a]	[27]	1967
68 ± 8[a]	[28]	1971
128[a]	[29]	1976
53 ± 10[a]	[13]	1977
60 ± 8[a]	[30]	1978
66[a]	[31]	1981
135[a]	[32]	2000
48.4[a]	[9]	2002
53.7[a]	[9]	2005
63 ± 4[a]	[9]	2008
62.3[b]	[10]	2016
66.06 ± 2.49	ENDF/B-VIII.0	2018
56.4 ± 5.0	this work	2024

[a]Read from Ref. [9].
[b]Theoretical calculation.

(6) Since the γ characteristic peaks of other de-excitation paths were not identified in this experiment, their error contribution is taken as 3.3%, based on their proportion reported in Ref. [17].

Overall, the primary sources of error include the statistical uncertainty of the characteristic γ rays. Additionally, the energy efficiency of the HPGe detector and the effects of other possible decay paths of ^{92}Zr cannot be ignored.

F. The calculation of MACS

In *s*-process nucleosynthesis studies, it is necessary to integrate the experimental neutron capture cross sections (n, γ) with the neutron velocity distribution in stellar plasma to calculate elemental abundances. This integration produces MACS, which are essential for accurate abundance calculations:

$$\langle \sigma \rangle_{kT} = \frac{\langle \sigma \upsilon \rangle}{\upsilon_T} = \frac{2}{\sqrt{\pi}} \frac{1}{(kT)^2} \int_0^\infty \sigma(E_n) E_n e^{-E_n/kT} dE_n. \quad (7)$$

This work calculated the MACS at a typical *s*-process temperature of $kT = 30$ keV and compared these values with those from other studies, as shown in Table II.

IV. RESULTS AND DISCUSSION

Most of the reaction cross sections obtained in this work are above 100 mb with a few data points around 20 mb. This is consistent with the magnitude of previous works. The uncertainty mainly comes from the statistical error of the data. The error in most of the cross section data is around 10%. For a few data points with very low cross sections, the errors exceed 30%. Figure 7 compares the data from this work with previous works and ENDF/B-VIII.0. As can be seen from the figure, the results measured in previous experimental works are generally smooth, with no significant oscillations even in the resonance region. However, the results from this work clearly show intense oscillation effects in the resonance region. The authors believe that the reason for this discrepancy lies in the fact that previous studies measured the combined effects of multiple reactions and then used theoretical methods to calculate the proportion of the yield from ^{91}Zr capturing neutrons, thereby determining the reaction cross section. Because it is the overall effect of multiple reaction cross sections, it masks the inherent characteristics of the neutron capture cross section, resulting in the oscillation effect not being well represented. In contrast, this work specifically measured the characteristic γ rays produced by the neutron capture reaction, without interference from other reactions, thus allowing for a better restoration of the original nature of the reaction.

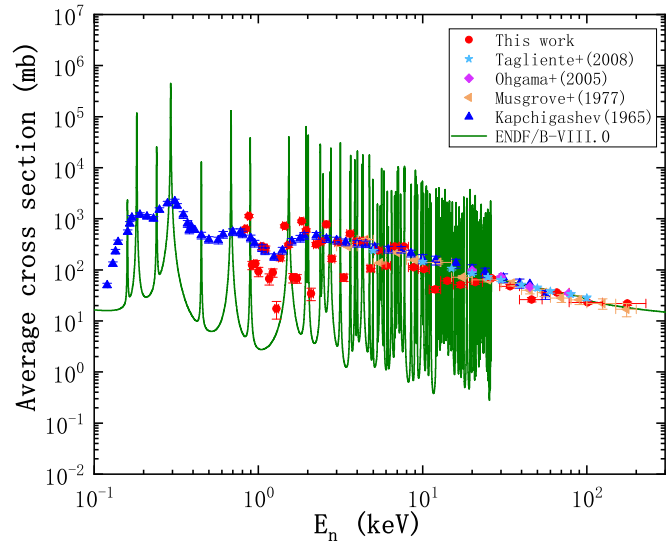

FIG. 7. The cross sections of ^{91}Zr$(n, \gamma)^{92}$Zr reaction with the neutron energy from 0.82 keV to 229 keV.

V. CONCLUSIONS

This study was conducted on the Back_n neutron beam line at CSNS. By bombarding a natural Zr metal target with white neutrons, the cross section for $n + ^{91}$Zr was measured. Unlike previous experiments, an HPGe detector with an extremely high γ energy resolution was employed to identify the characteristic γ rays at 912.7 keV and 934.5 keV. This allows for excluding the influence of other zirconium isotopes and other elements, such as oxygen, leading to a more convincing measurement of the reaction cross section. Notably, at neutron incident energies below 10 keV, we observed significant oscillatory effects in the measured cross sections, demonstrating that the measurement method employed in this work has significant advantages over previous approaches. In the nonoscillating region, the cross sections obtained in this work show agreement with the results of previous work within the margin of error. It provides a different perspective for measuring similar reactions. However, due to the lower detection efficiency of the HPGe detector compared to others like C_6D_6, considerably longer measurement times were required to ensure sufficient statistical accuracy.

In conclusion, this research not only provides detailed measurements of ^{91}Zr's neutron capture cross section but also sets

the stage for future studies that could explore similar measurements across different isotopes. Further research should consider the broader implications of these findings in astrophysics and nuclear physics.

ACKNOWLEDGMENTS

This work was performed with the support of the National Natural Science Foundation of China under Grants No. 12175152 and No. 62204162, the Guang dong Key Research and Development Program No. 2020B040420005, the Guang dong Basic and Applied Basic Research Foundation No. 2021B1515120027, the Ling Chuang Research Project of China National Nuclear Corporation No. 20221024000072F6-0002-7, the Nuclear Energy Development and Research Project No. HNKF202224(28), and the Characteristic Innovation Project of Universities in Guangdong Province No. 2022KTSCX313.

[1] E. M. Burbidge, G. R. Burbidge, W. A. Fowler, and F. Hoyle, Rev. Mod. Phys. **29**, 547 (1957).
[2] M. Lugaro, F. Herwig, J. C. Lattanzio, R. Gallino, and O. Straniero, Astrophys. J. **586**, 1305 (2003).
[3] F. Käppeler, R. Gallino, S. Bisterzo, and W. Aoki, Rev. Mod. Phys. **83**, 157 (2011).
[4] N. Prantzos, C. Abia, S. Cristallo *et al.*, Mon. Not. R. Astron. Soc. **491**, 1832 (2020).
[5] B. Pritychenko, J. Phys. G. Nucl. Part. **48**, 08LT01 (2021).
[6] M. Busso, D. Vescovi, S. Palmerini *et al.*, Astrophys. J. **908**, 55 (2021).
[7] S. Lanzi, S. Cristallo, F. Giacomini *et al.*, EPJ Web Conf. **279**, 06003 (2023).
[8] C. Sneden, J. J. Cowan, and R. Gallino, Annu. Rev. Astron. Astrophys. **46**, 241 (2008).
[9] G. Tagliente, P. M. Milazzo, K. Fujii *et al.*, Phys. Rev. C **78**, 045804 (2008).
[10] S. Dutta, G. Gangopadhyay, and A. Bhattacharyya, Phys. Rev. C **94**, 024604 (2016).
[11] V. Avrigeanu and M. Avrigeanu, Phys. Rev. C **96**, 044610 (2017).
[12] S. P. Kapchigashev, At. Energ. USSR **19**, 294 (1965).
[13] A. de L Musgrove, J. Boldeman, J. Allen, B. J. Harvey, and R. Macklin, Aust. J. Phys. **30**, 391 (1977).
[14] K. Ohgama, M. Igashira, and T. Ohsaki, J. Nucl. Sci. Technol. **42**, 333 (2005).
[15] D. A. Brown, M. B. Chadwick, R. Capote *et al.*, Nucl. Data Sheets **148**, 1 (2018).
[16] U. Abbondanno, G. Aertsb, H. Alvarezet *et al.*, Nucl. Instrum. Methods Phys. Res. A **521**, 454 (2004).
[17] C. M. Baglin, Nucl. Data Sheets **113**, 2187 (2012)
[18] Z. G. Wang, M. L. Liu, Y. H. Zhang *et al.*, Phys. Rev. C **89**, 044308 (2014).
[19] Q. An, H. Y. Bai, J. Bao *et al.*, J. Instrum. **12**, P07022 (2017).
[20] H. Yi, T. F. Wang, Y. Li, X. C. Ruan *et al.*, J. Instrum. **15**, P03026 (2020).
[21] J. Y. Tang, Q. An, J. B. Bai *et al.*, Nucl. Sci. Tech. **32**, 11 (2021).
[22] X. Li, Z. An, W. Jiang *et al.*, Eur. Phys. J. A **58**, 251 (2022).
[23] Y. H. Chen, G. Y. Luan, J. Bao *et al.*, Eur. Phys. J. A **55**, 1 (2019).
[24] Y. H. Chen, Y. J. Qiu, Q. Li, S. Tang *et al.*, Eur. Phys. J. A **60**, 63 (2024).
[25] C. A. Bertulani, Comput. Phys. Commun. **156**, 123 (2003).
[26] L. Gan, H. B. Sun, Z. H. Li *et al.*, Phys. Rev. C **97**, 064614 (2018).
[27] R. L. Macklin and J. H. Gibbons, Phys. Rev. **159**, 1007 (1967).
[28] B. Allen, J. H. Gibbons, and R. L. Macklin, Adv. Nucl. Phys. **4**, 205 (1971).
[29] J. Holmes, S. Woosley, W. Fowler, and B. Zimmerman, At. Data Nucl. Data Tables **18**, 305 (1976).
[30] A. de L. Musgrove, B. Allen, J. Boldeman, and R. L. Macklin, *Neutron Physics and Nuclear Data for Reactors and other Applied Purposes* (OECD, Paris, 1978), p. 449.
[31] M. Harris, Astrophys. Space Sci. **77**, 357 (1981).
[32] T. Rauscher and F.-K. Thielemann, At. Data Nucl. Data Tables **75**, 1 (2000).